IEEE Access
Multidisciplinary ⋮ Rapid Review ⋮ Open Access Journal

Received February 9, 2021, accepted February 16, 2021, date of publication February 19, 2021, date of current version March 1, 2021.

Digital Object Identifier 10.1109/ACCESS.2021.3060517

A 24 GHz Microwave Sensor With Built-in Calibration Capability Designed in MMIC Technology

ROBERT SMOLARZ, KAMIL STASZEK, KRZYSZTOF WINCZA, AND SLAWOMIR GRUSZCZYNSKI, (Member, IEEE)
Department of Electronics, AGH University of Science and Technology, 30-059 Kraków, Poland

Corresponding author: Kamil Staszek (kamil.staszek@agh.edu.pl)

This work was supported by the National Science Centre under Grant 2016/23/D/ST7/00481 and Grant 2016/22/E/ST7/00021.

ABSTRACT A microwave sensor realized in monolithic technology, intended for permittivity estimation with the use of a highly sensitive coupled-line section, is presented in this paper. It also contains a dedicated measurement circuitry realized as a five-port correlator, therefore, a simple scalar power measurement can be utilized to obtain vector signal corresponding to the measured material without the usage of an external vector network analyzer. To suppress systematic measurement errors arising from the manufactured circuit's imperfections it is equipped with an integrated calibration block, the parameters of which can be simply tuned with two biasing voltages. The sensor is calibrated following a recently reported procedure, which requires neither known nor specific calibration values, in contrast to other methods with much stronger constraints. It is shown for the first time, that a measurement system incorporating a multiport correlator can be successfully calibrated with such arbitrarily chosen settings of the calibration block. To experimentally validate correctness of the calibration's convergence, the developed sensor is calibrated multiple times with different sets of the calibration block's settings, each time resulting in the same output values. It proves that the approach to calibration of measurement systems incorporating the multiport correlator can be significantly simplified with no impact on calibration accuracy. Finally, the measurement of the sensor's response for two dielectric samples clearly demonstrates the advantages of the utilized calibration.

INDEX TERMS Calibration, correlators, directional couplers, monolithic microwave integrated circuits (MMICs), permittivity, sensors.

I. INTRODUCTION

Measurements of materials' physical properties are of great importance in contemporary both industrial and scientific area. In particular, measurements of permittivity in microwave frequency are ones of those frequently performed. Due to a large permittivity difference between water and dry fruits, vegetables or other matter, permittivity measurement provides a non-invasive and fast method used in agricultural industry for estimation of water content in soil [1], or in food products [2]–[4]. Similarly, such measurements are utilized for fat content determination in milk [5], [6], or glucose content in blood [7]. Recently, permittivity measurements have also been used to measure acetone content in exhaled human breath, where gas particles interact with gas-sensitive thin film, changing its permittivity [8]. It is a promising technique, since acetone has been recognized as a biomarker of diabetes [9], [10]. The currently developed systems are capable of a correct measurement even for as low gas concentration as less than 1 ppm [11].

An accurate measurement instrument has to contain two major components i.e., a sensitive sensor and a dedicated measurement circuitry. First component should respond with a possibly large change of one of its parameters. In case of permittivity measurement, a large variety of sensors has been proposed. Generally, they can be divided into two major groups: resonant sensors, and non-resonant ones, also called wideband. The resonant sensors change their resonant frequency along with the permittivity [12]. Such sensors exhibit a high sensitivity; however, they operate only at a certain frequency. Moreover, they require a precise tuning and frequency measurement. On the other hand, for

The associate editor coordinating the review of this manuscript and approving it for publication was Md. Abdur Razzaque.

non-resonant sensors permittivity can be inferred basing on a complex reflection or transmission coefficient over frequency [13], [14]. Hence, for each frequency of operation, a separate value of permittivity can be determined [14]. As shown in [11] a sensor's response measured over a wide bandwidth can also be used to enhance the sensitivity. In addition, such sensors are characterized by a simpler structure, being more robust e.g., to manufacturing intolerances [6].

As mentioned earlier, the second key component that always works in conjunction with the sensor is a measurement equipment. Nowadays, vector network analyzers (VNAs) are commonly used in all microwave laboratories. They can provide accurate measurements of scattering parameters over very wide bandwidth. Due to these reasons, in a great majority of reported research on microwave sensors, the vector network analyzer is used to measure the sensor's response [15]–[17]. Although VNA is suitable for laboratory environment, it is not an optimum measurement apparatus for mobile sensors, which should be compact, small, and low-cost. A typical VNA provides a large variety functions and features, which in sensor's application remain unused.

To simply the measurement circuitry to the minimum, with preserving its accurate measurement capabilities, a VNA can be replaced by a multiport correlator [18], [19]. It is a passive power distribution network, having two inputs and three (or more) outputs. The first input is fed with the measured signal, whereas to the second one a reference signal is connected. Due to an appropriate signal distribution in terms of both magnitude and phase, three (or more) output ports provide signals the power of which can be translated to the complex measured signal [20]. Therefore, using a simple circuitry and scalar power readings, complex scattering parameters can be measured. A great number of circuits utilizing multiport correlators have been presented in literature. The most common are reflectometers (composition of a correlator and an additional directional coupler) for complex reflection coefficient measurement [21], [22]. More sophisticated circuits having two measurement ports enabling measurements of both reflection and transmission coefficients are also reported [23]–[25]. They can operate at a single frequency or cover a very wide bandwidth [26]. Apart from the topology, these multiport measurement systems can be designed in microstrip [6], [19] or stripline technique, [20], [26], however, integrated solutions are also reported [27], [28].

In literature a number of multiport measurement systems intended for permittivity measurements has been reported. In [29] a wireless sensor is proposed, where a six-port correlator is used twice. Firstly, it serves for modulating the complex signal containing information on the measured dielectric sample at the sensor-modulator side. On the other hand, it is utilized as a demodulator in the receiver block. Another interesting example can be found in [30], where a six-port reflectometer is applied for determining moisture content of biomass material. On the other hand, in [31] a multi-state reflectometer is proposed, in which only two power detectors are used to determine permittivity of material under test. As a trade-off for decreased number of power detectors, a sequential power measurement for different adjustable short-circuits is required. In contrast, in [32] a multiport system capable of measuring both reflection and transmission coefficients is reported. It incorporates a coplanar permittivity sensor applied for measurements of aqueous glucose solutions.

In order to perform an accurate measurement each measurement system must be beforehand calibrated. A practical realization of a multiport correlator deviates from its ideal model, hence amplitude and phase imbalance occur, together with different power detectors sensitivity [33], [34]. These factors must be taken into account and compensated to suppress or eliminate systematic errors. A typical calibration is a process somehow opposite to actual measurement. To calibrate the measurement system, a set of well-defined and known a priori values, called calibration standards, must be measured. Then their genuine values and the corresponding measurement readouts can be used to determine the calibration constants, constituting a mathematical model of the system [25], [34], [35]. In such a procedure however, the measured component (e.g., sensor) has to be disconnected and replaced with calibration standards. This must be done in the systems like these reported in [30] and [32], where the sensing element is connected to the measurement circuitry with the aid of coaxial connectors. On the other hand, for calibrating the system presented in [31] an additional port is used for sequential measurement for eleven well-defined calibration standards.

It is clearly seen that the approach described above cannot be applied in systems, in which the measurement circuitry is integrated with the sensor, as its disconnection and replacement for calibration standards is not possible. Hence, an integrated system should be equipped with a built-in calibration block, which unfortunately does not allow for its separate characterization. As a consequence, only an approximate values of calibration standards are known, basing on electromagnetic simulation. Therefore, a calibration method involving unknown calibration standards can only be applied. For multiport correlators the most common calibration technique is based on the measurement of at least five calibration standards exhibiting unknown, but possible well-distributed phases, and unknown, but equal magnitudes [36]–[38]. This technique is relatively straightforward, and mathematically can be brought to derivation of five coefficients describing an ellipse on a complex plane, according to geometrical description of measurement using a multiport reflectometer [39].

Although the method described above is of relaxed calculation complexity it seriously suffers from the need of usage of at least five calibration constants of the same magnitude. This requirement becomes particularly difficult for systems operating at higher frequencies. An interesting example of a calibration block that can be built in the measurement system is shown in [40], where a quadrature directional coupler with eight biased diodes arranged along transmission lines are used to realize a phase shifter operating at 24 GHz.

As presented the magnitude of phase shifter's transmission coefficient S_{21} differs by more than 4 dB for different settings of the required phase shift. Such a magnitude deterioration impairs the calibration procedure convergence. To overcome this limitation, a recently reported calibration method can be used, which makes use of calibration standards characterized by unknown both magnitudes and phases [41]. Moreover, their magnitudes can differ. Such a solution greatly relaxes requirements related to the design of calibration blocks intended to be integrated with the measurement circuitry.

In this paper a novel microwave sensor for permittivity measurement at 24 GHz is proposed. A sensing element is realized as a coupled-line section, the transmission coefficient of which changes along with the permittivity of the tested material. To measure the coupled-line section's response a five-port reflectometer is introduced. Moreover, to suppress the measurement circuitry imperfections a calibration block is also built in the sensor. The presented sensor has been designed in PH25 process from United Monolithic Semiconductors (UMS) and manufactured. Additionally, its particular components have been manufactured as separate components on the same substrate for verification purposes. The scattering parameter measurement done with a vector network analyzer confirm good performance of these components. Finally, the calibration block has been utilized to calibrate the developed sensor with the calibration method reported recently in [41], with the use of unknown calibration standards. For the very first time a calibration of a multiport correlator-based sensor with integrated calibration block is reported, in which unknown calibration standards having different magnitudes and phases are used. The obtained results exhibit no difference over a large number of the utilized calibration standards' combinations, which proofs the calibration correctness. It also confirms that the requirements on integrated calibration blocks can be relaxed, as the calibration standards can be of different magnitudes and phases simultaneously. To show the advantage of the introduced built-in capability two dielectric samples were measured. The obtained response of the calibrated sensor is close to the corresponding measurements performed with a vector network analyzer.

II. DESCRIPTION OF THE PROPOSED MICROWAVE SENSOR

A general block diagram together with detailed schematic diagrams of its particular components are presented in Fig. 1. The entire sensor constitutes a four-port structure fed at port #1, whereas to the remaining ports #2 – #4 three power detectors are connected. Its principle of operation can be described as follows. The microwave signal delivered to port #1 is equally split by the power divider PD_1 into two identical signals. The signal from port $\#2_D$ excites the coupled-line section, which serves as a sensing element of the proposed sensor. As can be observed to the coupled-line section two baluns are connected, which ensure odd excitation of the section, as described in [6]. Such an excitation provides high

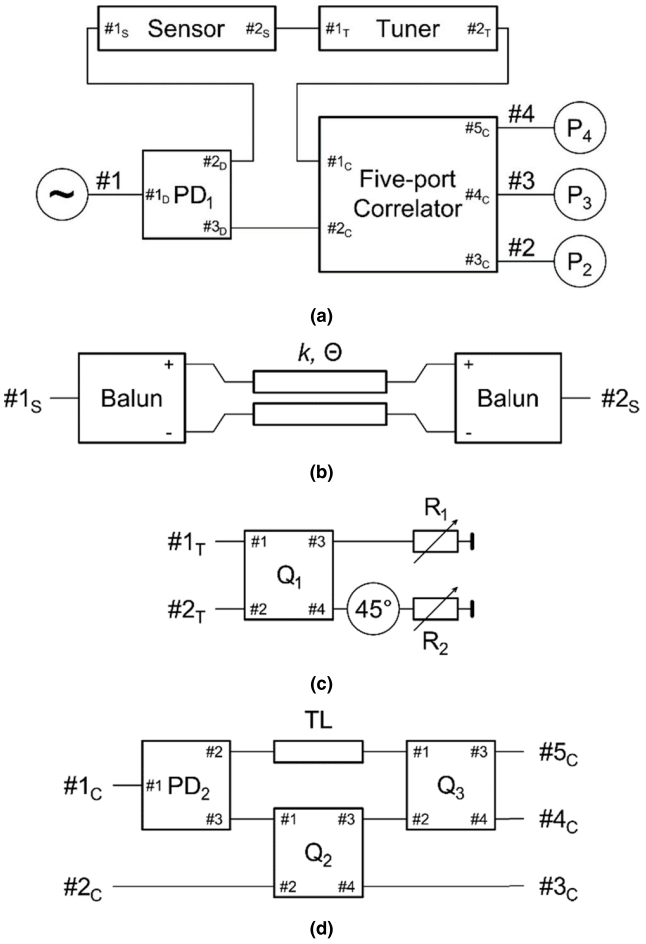

FIGURE 1. Block diagram of the presented sensor (a) and detailed schematic diagrams of particular components: coupled-line section (b), calibration tuner (c), and five-port correlator (d).

density of electromagnetic field in a close proximity along the gap between two coupled lines [42]. A disturbance of the mentioned field caused by placing a material under test on the coupled-line section leads to a change of its transmission coefficient S_{21}^S, therefore, by the measurement of the sensor's complex transmission coefficient the electrical properties (effective permittivity) of the material under test can be estimated. It is worth mentioning that due to advantageous distribution of the electromagnetic field, the application of the sensor of the above-described topology provides significantly higher sensitivity than e.g., sensors constructed as a transmission line [42].

In order to measure the complex transmission coefficient of the coupled-line section S_{21}^S, the proposed sensor has been equipped with a five-port correlator, reported previously in [6]. It is fed with two signals. First of them is the signal that propagates through a cascade formed by the coupled-line section and a calibration tuner presented in Fig. 1(c), and is delivered to port $\#1_C$ of the correlator. This signal is a subject to measure in order to estimate effective permittivity of material under test placed onto the coupled-line section. The calibration tuner during measurement provides transmission coefficient S_{21}^T between its ports $\#1_T$ and $\#2_T$, which

is constant during the measurement, hence it has no impact on the measurement. It is, however introduced for sensor's calibration purpose, which is described in the next section.

The second input port #2$_C$ of the five-port correlator is fed with the signal directly from port #3$_D$ of the power divider PD$_1$. This signal, named I_{REF}, serves as a reference and is not affected by the measured material. The correlator provides three output signals at ports #3$_C$ – #5$_C$, being also the output ports of the entire sensor i.e., ports #2 – #4, respectively, to which three power detectors are connected. As it is shown in the next section the power values $P_2 - P_4$ measured by these three power detectors can be translated to the complex signal dependent on the physical properties of the material under test placed onto the coupled-line section.

It can be observed that the proposed sensor is similar to the system reported in [6]. There are, however, some substantial differences. First, the proposed sensor is equipped with the calibration tuner, which as it will be shown in the next section allows for calibration of the sensor i.e., for elimination of systematic errors resulting from imperfect match and isolation of the particular components, or different sensitivity of the applied power detectors P$_2$ – P$_4$. Further differences are in the frequency of operation and technology of realization. The proposed sensor has been designed and manufactured in MMIC technology, and its operational frequency has been increased to 24 GHz, whereas the system reported in [6] has been designed in microstrip technique with the use of Arlon 25N laminate and designated for much lower frequency of 2.4 GHz. Additionally, the proposed system has been designed with the use of lumped LC elements, which has allowed for a significant size reduction. As a consequence, much lower volume of material under test is needed to perform a measurement comparing to the system reported in [6], in which the measurement cell has a volume of 2.75 ml. More detailed description of the sensor system design will be given in Section IV.

III. CALIBRATION & MEASUREMENT CAPABILITY

As indicated in the previous section, the presented sensor is equipped with a five-port correlator allowing for the measurement of the complex S_{21}^S signal related to the effective permittivity of material under test with the use of three power measurements. Hence, by simple scalar measurement of power, a vector measurement allowing for estimation of the measured material's permittivity can be realized with the use of the proposed sensor. Additionally, the sensor also contains the calibration tuner, which can be used to eliminate systematic measurement error arising from non-ideal impedance match and isolation of the particular components constituting the proposed sensor.

The five-port correlator seen in Fig. 1(d) is composed of an equal-split power divider PD$_1$, a 4.77 dB/90° directional coupler Q$_2$, a 3 dB/90° directional coupler Q$_3$, and a section of transmission line TL [6]. Assuming ideal impedance match and isolation of all the mentioned components, the five-port correlator can be described by the following scattering matrix:

$$S^C = \frac{1}{\sqrt{3}} \begin{bmatrix} 0 & 0 & e^{j\frac{\pi}{2}} & e^{j\frac{\pi}{6}} & e^{j\frac{\pi}{3}} \\ 0 & 0 & e^{-j\frac{\pi}{2}} & e^{j\frac{\pi}{2}} & e^{j0} \\ e^{j\frac{\pi}{2}} & e^{-j\frac{\pi}{2}} & 0 & 0 & 0 \\ e^{j\frac{\pi}{6}} & e^{j\frac{\pi}{2}} & 0 & 0 & 0 \\ e^{j\frac{\pi}{3}} & e^{j0} & 0 & 0 & 0 \end{bmatrix} \quad (1)$$

Therefore, the power $p_2 - p_4$ measured at ports #2 – #4 and normalized by the power delivered from the signal source to port #1 P_{GEN} can be expressed as:

$$p_2 = \frac{P_2}{P_{GEN}} = \left| S_{32}^C I_{REF} + S_{31}^C I \right|^2 = q_2 \left| c_2 I_{REF} - I \right|^2 \quad (2)$$

$$p_3 = \frac{P_3}{P_{GEN}} = \left| S_{42}^C I_{REF} + S_{41}^C I \right|^2 = q_3 \left| c_3 I_{REF} - I \right|^2 \quad (3)$$

$$p_4 = \frac{P_4}{P_{GEN}} = \left| S_{52}^C I_{REF} + S_{51}^C I \right|^2 = q_4 \left| c_4 I_{REF} - I \right|^2 \quad (4)$$

where I is the signal that propagates through the coupled-line section and the calibration tuner:

$$I = S_{21}^S \cdot S_{21}^T \quad (5)$$

and the coefficients q_i and c_i ($i = 2, 3, 4$) are equal to:

$$q_2 = q_3 = q_4 = \frac{1}{3} \quad (6)$$

$$c_2 = 1 \quad (7)$$

$$c_3 = \frac{-1 - j\sqrt{3}}{2} \quad (8)$$

$$c_4 = \frac{-1 + j\sqrt{3}}{2} \quad (9)$$

By solving the set of equations (2) – (4) with the coefficients having values as indicated in (6) – (9) the signal I_N, being the signal I normalized by the reference signal I_{REF}, can be found:

$$I_N = \frac{I}{I_{REF}} = -P_2 + \frac{1}{2}P_3 + \frac{1}{2}P_4 + j\frac{\sqrt{3}}{2}(P_3 - P_4) \quad (10)$$

where

$$I_N = S_{21}^S \cdot \frac{S_{21}^T}{I_{REF}} \quad (11)$$

As given by (10), the complex signal related to the measured material's permittivity can be found by simple scalar measurement of three power values. The equation (10), however, holds only for ideal values of the coefficients q_i and c_i. In practical realization these values deteriorate, therefore, their actual values have to be found prior to the measurement. For this purpose, the calibration tuner shown in Fig. 1(c) can be utilized. It is composed of a 3 dB/90° directional coupler Q$_1$, a 45°-phase shifter and two variable resistors R$_1$ and R$_2$ connected to the ground plane. As seen the presented tuner is a simplified version of the programmable two-port with varying scattering parameters (both reflection and transmission coefficient) reported in [43], in which however, each variable resistance has been realized as a

cascade connection of programmable attenuator and SPDT (single pole double throw) switch, with one output port opened, and the second one shorted to the ground. In contrast, in the proposed sensor, the variable resistances have been realized with the use of two pHEMT transistors, the drain-source resistances of which are controlled by biasing voltages. As a consequence, much simpler and more compact circuitry has been used, which also allows for high frequency operation.

A classic calibration in general is a procedure being opposite to the measurement. It requires measurement of several known samples, called calibration standards, and reading the corresponding power values. Then, by knowing the relation between the measured value and the measured power (2) – (4), the coefficients q_i and c_i can be calculated and taken into account in derivation of the measured signal I_N. Such a calibration approach is straightforward, however, in practice it would require exchanging the coupled-section implemented in the sensor for other components having known scattering parameters, which is not possible. Another method could make use of the measurement of several materials of known parameters placed on the coupled-line section. This calibration method however, is sensitive to the material samples placement accuracy and occurrence of air gaps between the material and the coupled-lines. Therefore, in the presented sensor a dedicated built-in calibration tuner has been implemented.

As indicated in (11), the calibration tuner's transmission coefficient S_{21}^T influences the measured signal I_N identically as the transmission coefficient of the coupled-line section S_{21}^S. Thus, by tuning S_{21}^T, which is done by applying variable voltages to the gates of pHEMT transistors realizing resistances R_1 and R_2, one can obtain power values that would be obtained by placing different material samples on the coupled-line sections. It is worth mentioning that the developed tuner can also provide $S_{21}^T = 0$, which can be additionally useful. The power values obtained for corresponding values of the tuner's transmission coefficient S_{21}^T can be used in the calibration procedure reported in [41]. This procedure allows determining the parameters describing the sensor i.e., q_i and c_i with the use of the power values measured for several unknown values of the transmission coefficient S_{21}^T, and for $S_{21}^T = 0$. It is worth underlining that due to analog control of the pHEMT transistors realizing the resistors R_1 and R_2, a large number of different values of S_{21}^T can be obtained, including zero. It is also worth noting that although the calibration method described in [41] utilizes unknown calibration standards, they should be distinctly distributed over the complex plane i.e., they should differ in both magnitude and phase, to ensure good robustness. Such selection of the values of S_{21}^T can be done via electromagnetic simulation, since only a coarse information of the S_{21}^T values is needed. Hence, basing on the simulation, a required number of biasing voltages of the pHEMT transistors can be selected, and then used in the calibration of the manufactured sensor.

IV. SENSOR DESIGN IN MMIC TECHNOLOGY

The proposed sensor has been designed in a monolithic technology, PH25 process based on gallium arsenide (GaAs) offered by UMS. The process is intended for usage in low-noise applications operating up to 40 GHz, and contains components such as pHEMT 0.25 μm transistors, diodes, MIM capacitors, spiral inductors and different types of resistors. Furthermore, the PH25 allows for using three metallization layers, which can be useful in design of complex passive structures.

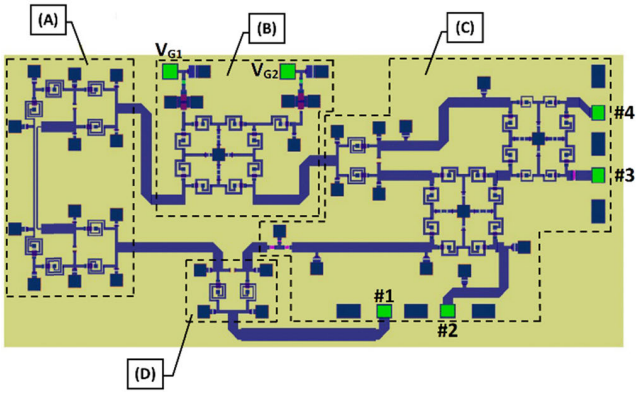

FIGURE 2. The general view on the monolithic sensor designed in the UMS PH25 process. The following functional blocks can be distinguished in the picture: coupled-line section (A), voltage-controlled calibration tuner (B), five-port correlator (C), and Wilkinson power divider (D).

Fig. 2 presents the designed integrated sensor based on the conception shown in the Fig 1, operating at the center frequency of 24 GHz. The following components can be noticed in the 2D view i.e., the coupled-line section with two balanced-unbalanced circuits (baluns) (A), the voltage-controlled calibration tuner (B), the five-port correlator (C), and the Wilkinson power divider PD_1 (D). One of the most crucial aspects in a monolithic technique design is related to miniaturization. Thus, to decrease size of passive components such as couplers, power dividers, and transmission lines, they have been designed utilizing lumped elements. Such an approach significantly reduces circuit's dimensions, however an increase of losses has to be taken under consideration during the design process.

A sensing part of the sensor is shown in Fig. 3. It is composed of a coupled-line section (A) and two balanced-unbalanced (baluns) marked as (B). The coupled lines have 8 μm width, 3 μm thickness, and the spacing between them is equal to 8 μm. The total length of the coupled section is 570 μm. As seen geometry of the structure enables measurements of biological and chemical samples in micro-scale. To maximize the sensor's sensitivity to tested materials' permittivity, an odd excitation of the coupled section needs to be applied, which has been realized with two identical baluns (B). A single circuit is composed of an equal-split Wilkinson power divider and phase shifter which ensures 180° differential phase between the balun's output signals. Fig. 4 presents a closer view on the utilized balun with marked

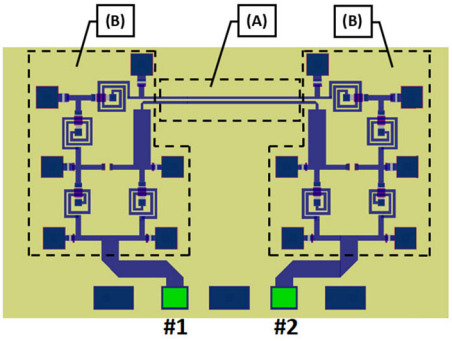

FIGURE 3. 2D view of the sensing part consisting of coupled-line section (A) and two baluns circuits (B).

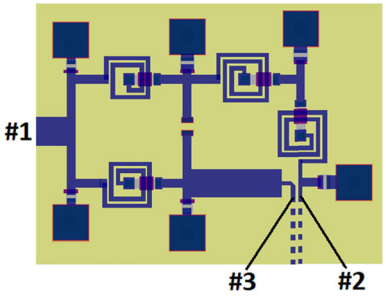

FIGURE 4. Detailed 2D view of the designed balun circuit.

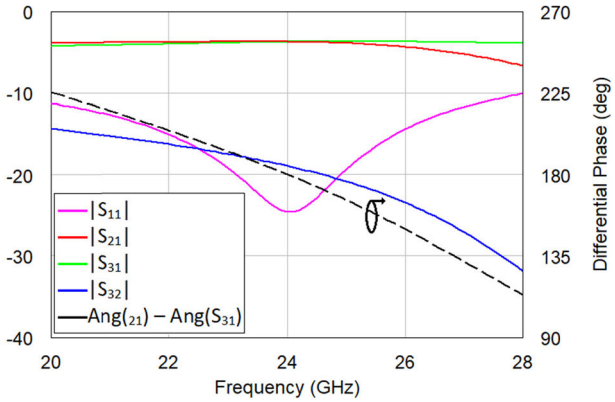

FIGURE 5. Scattering parameters of the designed baluns. Results of electromagnetic simulation.

ports, whereas Fig. 5 shows S-parameters and differential phase obtained during electromagnetic simulation.

Next functional block of the presented sensor is the calibration tuner illustrated in Fig. 1(c). It is composed of an equal split-quadrature coupler, a 45° phase shifter, and two variable resistances. A 2D view of the designed component is shown in Fig. 6. The directional coupler has been realized in branch-line topology (A) and the phase shifter has been designed as a simple LC circuit (C). To realize the variable resistances R_1 and R_2 of the tuner, two 75 μm two-finger gate pHEMT transistors (B) have been applied. Their drain-source resistance realizing the mentioned resistances can be controlled by external biasing voltages, as it is shown in Fig. 7. It can be observed that the biasing voltage from −0.8 V

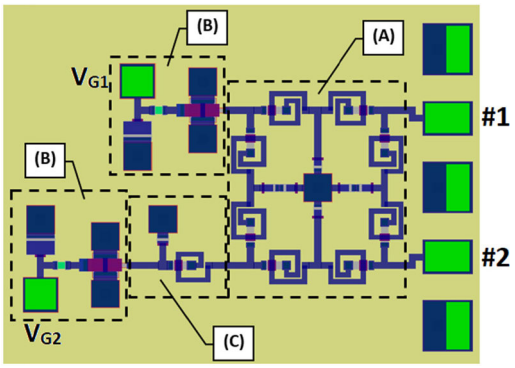

FIGURE 6. 2D view of the calibration tuner. The following circuits can be noticed in the picture: branch-line coupler (A), pHEMT transistors with biasing circuits (B), and 45° phase shifter (C).

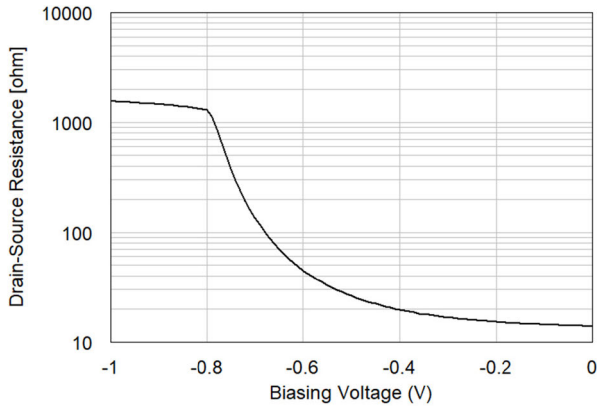

FIGURE 7. Drain-source resistance of pHEMT transistor vs. biasing voltage. Simulated values obtained for 75 μm two-finger gate pHEMT transistor.

to 0 V provides a wide range of resistance, which in turn will ensure broad range of the calibration tuner's transmission coefficient S_{21}^T values needed for robust calibration of the presented integrated sensor.

The calibration tuner has two independent identical biasing circuits – one for each transistor. To set proper values of these voltages, external supplies have to be connected to the pads V_{G1} and V_{G2} seen in Fig. 6. The maximum spread of the tuner's transmission coefficient S_{21}^T has been examined with the use of a simulation performed for different biasing voltages both ranging from −0.8 V to 0 V with the step of 10 mV. Further, similar procedure has been performed for the manufactured tuner, however, with the step increased to 100 mV. The obtained results are presented in Fig. 8. As seen the simulated and measured distributions of the presented transmission coefficients are similar. Moreover, it can also be noticed that the tuner exhibits relatively wide tuning range, which is crucial for further calibration of the integrated sensor.

The final component of the presented sensor is the five-port correlator illustrated in Fig. 1(d). Its design is presented in Fig. 9. This circuit contains four basic components i.e., the branch-line couplers (A) and (B) which have 3 dB and 4.77 dB coupling, respectively, the 3 dB Wilkinson

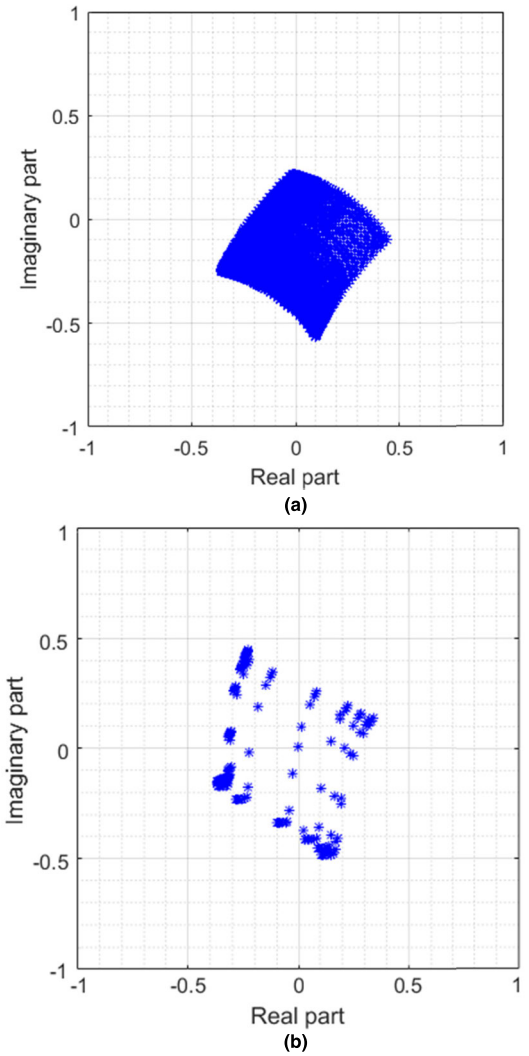

FIGURE 8. Distribution of the developed calibration tuner's transmission coefficient S_{21}^{T}. Results of electromagnetic simulation (a) and measurements of the manufactured tuner (b).

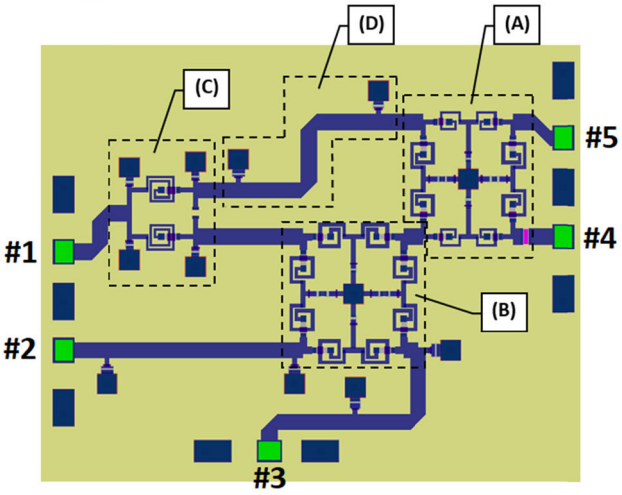

FIGURE 9. 2D view of the five-port correlator. The following circuits can be noticed in the picture: 3 dB branch-line coupler (A), 4.77 dB branch-line coupler, Wilkinson power divider (C), and quarter-wave transmission line (D).

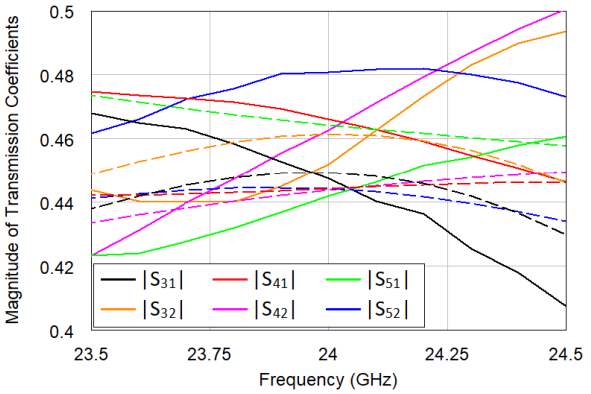

FIGURE 10. Magnitude of simulated (dashed lines) and measured (solid lines) transmission coefficients of the developed five-port correlator.

power divider (C), and the quarter-wave transmission-line (D). To achieve such an electrical length under the overall dimensions constrains, the transmission-line has been shortened physically with the aid of two capacitors. According to the theoretical analysis given in Section III together with the mathematical model (1), the five-port correlator should exhibit an equal division of the signal from each input ports i.e., $\#1_C$ and $\#2_C$ to all output ports $\#3_C - \#5_C$, simultaneously providing for each output port 120°, −120° or 0° of phase shift for signals delivered to the input ports. To verify the above properties, the scattering parameters of the electromagnetically simulated correlator, together with the measurement results of the fabricated correlator are depicted in Fig. 10 and Fig. 11. As can be seen the obtained results clearly correspond to the theoretical assumptions, allowing for measurements with the developed sensor at the center frequency of 24 GHz, according to the investigation given in Section III. However, to completely eliminate the impact of the observable imperfections, a calibration procedure is required.

The overall view of the fabricated integrated sensor is presented in Fig. 12. The die can be divided into two parts, where top one is the complete sensor, and the bottom one contains the coupled-line section, the calibration tuner and the five-port correlator fabricated as separate circuits for experimental verification. The manufactured die has dimensions 3.4 mm × 4.0 mm. It is also worth noting that all the elements on chip are exposed, as the utilized PH25 process by UMS does not provide a passivation coating on the top metallization layer. It increases the sensor's sensitivity, as the material under test can be placed closer to the coupled lines, where the electromagnetic field is the highest. It also allows e.g., for selective deposition of a thin film that changes its permittivity under a target gas exposure onto the coupled-line section, being the sensing element, as reported in [8], and [11]. On the other hand, the absence of the top protecting layer obviously makes the manufactured die more prone to a damage. Nevertheless, if a relatively small damage occurs, that deteriorates the circuit's electrical parameters, the entire sensor can be calibrated again, to eliminate the new source of

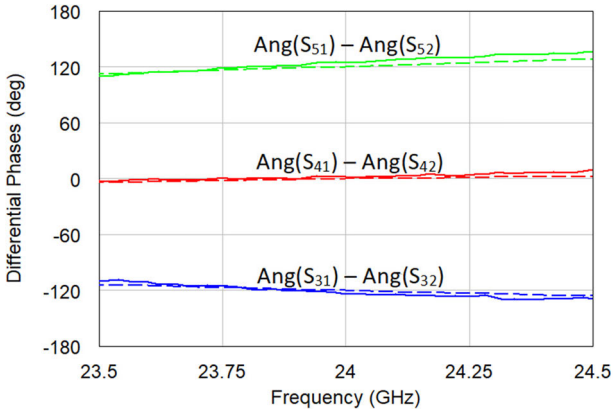

FIGURE 11. Simulated (dashed lines) and measured (solid ones) differential phases of the developed five-port correlator.

a systematic error. Moreover, the sensor can be periodically calibrated to compensate any long-term drifts.

V. CALIBRATION OF THE MANUFACTURED SENSOR

As presented in the above section, the developed calibration tuner provides a wide range of its transmission coefficient S_{21}^T, which can be used for calibration purpose. According to the calibration method reported in [41] at least eight different values of S_{21}^T and an additional setting ensuring $S_{21}^T = 0$ are needed. These values can be unknown, however, to ensure good performance, they should cover possibly large area on the complex plane i.e., they should differ in both magnitude and phase. To coarsely select the calibration standards, the calibration tuner manufactured as the separate circuit shown in Fig. 6 has been used. Moreover, since in actual calibration the other tuner, namely the one integrated in the sensor, is to be used, the manufacturing reproducibility should be examined. Therefore, a set of twelve different values of S_{21}^T has been selected together with $S_{21}^T = 0$. The corresponding gate voltages of transistors realizing the resistances R_1 and R_2 in the tuner have been applied to three manufactured calibration tuners. The obtained values of S_{21}^T measured with the use of a vector network analyzer are illustrated in Fig. 13. As can be seen these values are consistent, and the voltages ensuring S_{21}^T equal to zero for the first tuner, applied for the remaining two tuners provide S_{21}^T not exceeding -28 dB of magnitude. Such good convergence confirms a high manufacturing reproducibility and allows for statement that these values will be similar for the tuner integrated in the sensor, if the same biasing voltages are applied. Nevertheless, it should be emphasized that the integrated tuner does not have the output ports serving for measurement purposes as the tuners manufactured as separate circuits. Due to this fact a distinct difference, particularly in the phase of the selected values of S_{21}^T should be expected.

For the final stage of the experimental verification of the manufactured sensor, its all four ports were connected to the vector network analyzer N5224A by Keysight with the use of two GSGSG probes used previously to characterize

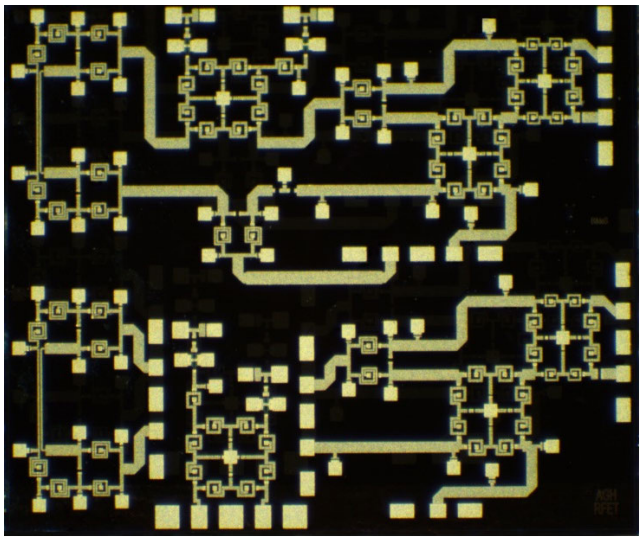

FIGURE 12. Picture of the manufactured die consisting of the complete sensor (top part) and its particular components (bottom part) i.e., coupled-line section, calibration tuner, and five-port correlator.

all manufactured components as described in Section IV. Although the vector network analyzer is capable of multiport measurements of complex signals, in the considered verification it was used for scalar power measurement, hence solely the magnitude measurements were utilized. Therefore, three measurements of signals' magnitudes, namely $|S_{21}^k|$, $|S_{31}^k|$, and $|S_{41}^k|$, were taken to obtain the normalized power readings:

$$p_2^k = \frac{P_2^k}{P_{GEN}} = \left|S_{21}^k\right|^2 \tag{12}$$

$$p_3^k = \frac{P_3^k}{P_{GEN}} = \left|S_{31}^k\right|^2 \tag{13}$$

$$p_4^k = \frac{P_4^k}{P_{GEN}} = \left|S_{41}^k\right|^2 \tag{14}$$

measured for each of $K = 13$ settings of the calibration tuner demonstrated in the previous section, for which the calibration tuners manufactured as separate circuits exhibit transmission coefficients S_{21}^T as shown in Fig. 13 ($k = 1, 2, \ldots, 13$).

The above values p_2^k, p_3^k, and p_4^k have been used to calibrate the manufactured sensor according to the method reported in [41]. It should be emphasized that since this method makes use of unknown calibration standards, it normalizes all values to the value of the first calibration standard. As a consequence, the measured values e.g., can have magnitudes greater than unity, even if a passive component is measured. Nevertheless, such normalization uniformly transforms all measurements, hence they all preserve mutual magnitude and phase relations. To verify the impact of calibration standards' selection on the calibration results, 26 different sets of them have been formulated. Each set contains the measurement corresponding to $S_{21}^T = 0$, and from 8 to 12 non-zero S_{21}^T settings. These sets can be summarized as follows:

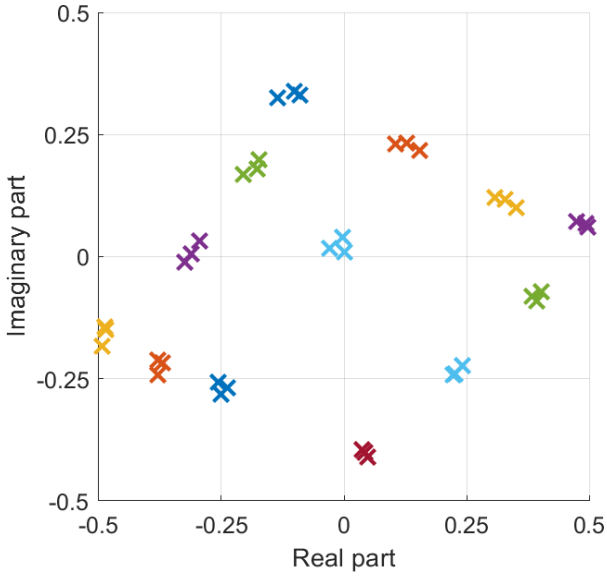

FIGURE 13. Twelve values of the calibration tuner's transmission coefficient S_{21}^T selected as calibration standards and zero transmission coefficient measured for three manufactures sensors to experimentally verify sensor's reproducibility.

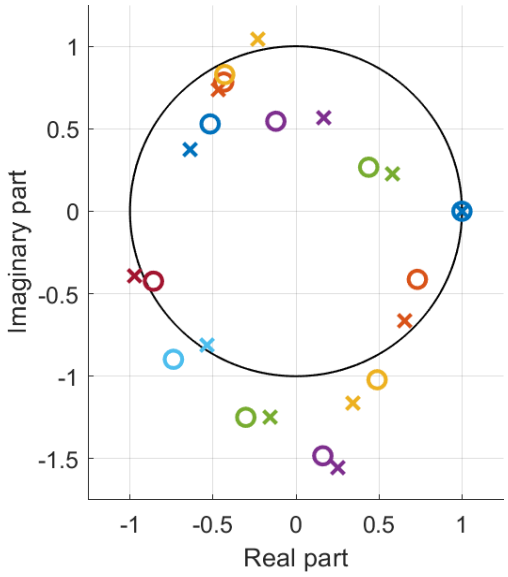

FIGURE 14. Calculated values of the signal I_N (o) obtained for twelve different settings of the calibration tuner compared to the transmission coefficient values of the calibration tuner manufactured as a separate circuit, measured for the corresponding settings (×).

1) 3 different sets composed of 8 non-zero S_{21}^T settings and a single setting for $S_{21}^T = 0$,
2) 4 different sets composed of 9 non-zero S_{21}^T settings and a single setting for $S_{21}^T = 0$,
3) 6 different sets composed of 10 non-zero S_{21}^T settings and a single setting for $S_{21}^T = 0$,
4) 12 different sets composed of 11 non-zero S_{21}^T settings and a single setting for $S_{21}^T = 0$,
5) single set composed of 12 non-zero S_{21}^T settings and a single setting for $S_{21}^T = 0$.

For all the above sets the calibration has been performed, obtaining 26 calibration results. Further, for each of these calibration results, the twelve sets of the same power values p_2^k, p_3^k, and p_4^k have been used to calculate the measured signal I_N given by (10) and (11), which are shown in Fig. 14. It must be underlined that regardless of the selected set of calibration standards, the obtained results are identical and are indistinguishable from each other, which proofs a high robustness of the calibration performed for the developed sensor. Moreover, the obtained values are compared to the corresponding transmission coefficients of the calibration tuner measured separately (shown in Fig. 13) normalized to the first one. It can be observed that both results shown good agreement. There are, however, distinct discrepancies, the results of which are twofold. First, the determined signal I_N takes into account the coupled-line section connected in cascade with the calibration tuner in the integrated sensor, therefore, both insertion losses and imperfect impedance match of the mentioned coupled-line section are expected to deteriorate slightly the final values of I_N. Secondly, the signal I_N are compared against the values measured for the calibration tuner manufactured as a separate circuit, therefore, equipped with additional sections of transmission lines and pads for GSGSG probes connection, which do not exist in the sensor with integrated calibration tuner. Again, imperfections of the mentioned pads manifest themselves in the difference between the results obtained for the considered circuits. In the light of the above it can be stated that the values of I_N are calculated correctly, however they inherently differ for the sensor with the integrated tuner, with respect to the S_{21}^T values of the calibration tuner manufactured as a separate circuit.

VI. EXPERIMENTAL VERIFICATION OF THE CALIBRATED SENSOR

For an experimental verification showing the calibrated sensor's response, namely the signal I_N, to DUT permittivity, two thin microwave laminates have been used. The first one is CuFlon, characterized by permittivity 2.08 and the thickness of 3 mils. As the second sample 4-mil thick Kapton laminate, having permittivity equal to 3.38 has been utilized. Since the coupled-line section being the sensing element is relatively small, as its length equals 470 μm, each sample has been cut out to a triangle shape, to easily adjust the sample's width to the coupled-line section's length. To precisely cover the entire coupled-line area with the tested sample of laminate a 3D millimeter positioner was used, as illustrated in Fig. 15. Due to relatively low permittivity of both samples, the signal I_N is expected to have low (negative) angle, however, the absolute value of the angle for Kapton should be higher than for CuFlon, according to their permittivity. On the other hand, the magnitudes should be close to unity, as these samples exhibit low losses.

The measurement for each sample was taken in three ways:

1. The sample was put to cover the coupled-line section in the manufactured sensor, the three power readings

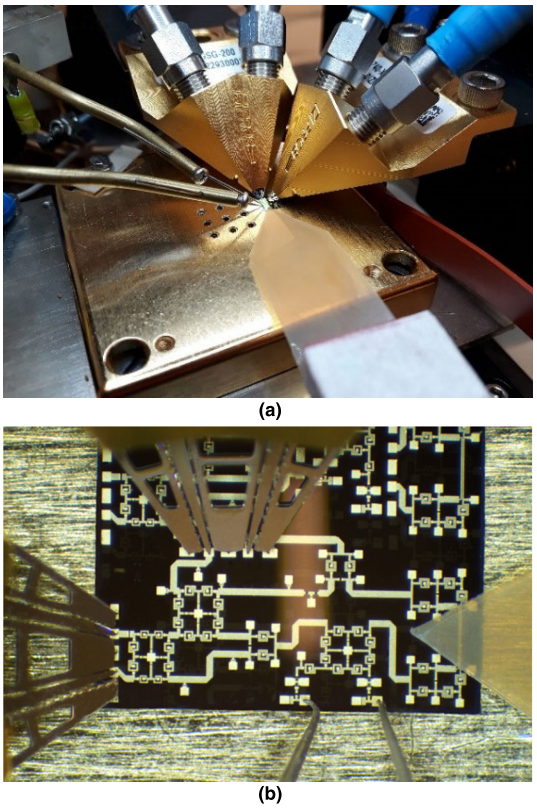

FIGURE 15. The measured dielectric sample (thin microwave laminate) on the coupled-line section: general view (a) and top view from microscopic camera (b).

$P_2 - P_4$ were measured and used as input data to the calibration algorithm described in Section 4,

2. As above, the sample was put to cover the coupled-line section in the manufactured sensor, the three power readings $P_2 - P_4$ were measured and used to calculate the signal I_N according to the formula (10) – hence no calibration was used,
3. The sample was put to cover the coupled-line section manufactured as the separate circuit seen in the bottom-left corner in Fig. 12, and its transmission coefficient S_{21} was measured directly by vector network analyzer N5224A by Keysight.

Furthermore, the measurement uncertainty has also been determined. For the VNA measurements it has been calculated with the aid of *Downloadable Vector Network Analyzer Uncertainty Calculator* provided by Keysight. The uncertainty for the measurements done with the use the calibrated five-port correlator has been estimated following the worst-case analysis reported in [44], that incorporates the power distribution scheme of the five-port correlator and the power measurement uncertainty. Since the VNA was used for $P_2 - P_4$ power measurement in the developed sensor, the utilized VNA's magnitude measurement uncertainty has been used as the power measurement uncertainty. Moreover, the uncertainty for the measurements done with a non-calibrated five-port correlator following the simplified formula (10) is

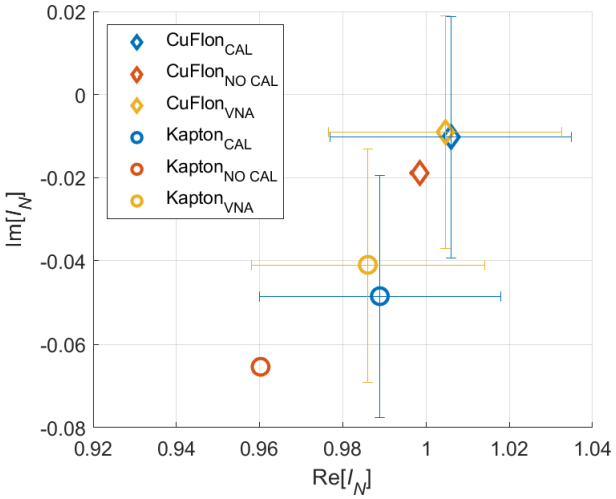

FIGURE 16. The signal I_N measured with the manufactured sensor for CuFlon and Kapton laminates, with the use of the calibration (CAL) and using the approximate formula (10) (NO CAL), compared to the corresponding transmission coefficients of the coupled-line section with balun manufactured as the separate circuit, measured directly with the aid of VNA (VNA).

undefined, since power distribution scheme in the measurement system remains unknown.

The obtained results are depicted in Fig. 16. As seen the measured values meet the theoretical expectations. Moreover, the values obtained for the calibrated sensor are definitely closer to the transmission coefficients of the coupled-line section covered with the samples measured directly using VNA, than the values calculated using the approximate formula (10), which do not take into account any deterioration of the manufactured circuit's parameters. The visible misalignment is most probably caused by limited precision of the dielectric samples' placing on the coupled-line section. Nevertheless, the performed test clearly shows the advantage of the built-in calibration capability of the developed sensor.

VII. CONCLUSION

In this paper, a new permittivity sensor integrated with the calibration block and a five-port correlator has been presented, and a novel approach to calibration has been proposed. The presented circuitry has been realized as a monolithic microwave integrated circuit operating at the frequency of 24 GHz. The sensing circuitry has been designed as a coupled-line section, the feeding of which maximizes it sensitivity to relative permittivity of the material to be tested. The sensor has been equipped with the five-port correlator allowing for an easy measurement of the complex signal proportional to the tested material's permittivity, through scalar power measurement. In order to suppress the systematic measurement errors a new approach to calibration has been proposed. It utilizes the calibration tuner connected in cascade with the coupled-line section, easily controlled by two voltages applied to pHEMT transistors' gates. As proven experimentally, the sensor is suitable for application of the recently reported calibration procedure, in which restrictions

related to calibration standards are significantly reduced with respect to other published solutions. The calibration has been verified for a large number of different sets of the tuner's settings, each time providing identical results. The obtained results clearly show that design of calibration blocks intended to integrate in such systems can be significantly simplified with respect to already published ones, since their parameters can be of arbitrary and unknown both magnitude and phase. For an additional confirmation the sensor's response has been measured for two dielectric samples with and without calibration. It is clearly seen that the application of the built-in calibration capability significantly enhances the quality measurement results.

ACKNOWLEDGMENT

The authors would like to thank UMS Foundry team for their substantive support during design process and fabrication.

REFERENCES

[1] A. Lewandowski, A. Szypłowska, A. Wilczek, M. Kafarski, J. Szerement, and W. Skierucha, "One-port vector network analyzer characterization of soil dielectric spectrum," *IEEE Trans. Geosci. Remote Sens.*, vol. 57, no. 6, pp. 3661–3676, Jun. 2019.

[2] S. Trabelsi and S. O. Nelson, "Microwave sensing of quality attributes of agricultural and food products," *IEEE Instrum. Meas. Mag.*, vol. 19, no. 1, pp. 36–41, Feb. 2016.

[3] S. Trabelsi, A. W. Kraszewski, and S. O. Nelson, "A microwave method for on-line determination of bulk density and moisture content of particulate materials," *IEEE Trans. Instrum. Meas.*, vol. 47, no. 1, pp. 127–132, Feb. 1998.

[4] S. Ryynänen, "The electromagnetic properties of food materials: A review of the basic principles," *J. Food Eng.*, vol. 26, no. 4, pp. 409–429, Jan. 1995.

[5] W. Guo, X. Zhu, H. Liu, R. Yue, and S. Wang, "Effects of milk concentration and freshness on microwave dielectric properties," *J. Food Eng.*, vol. 99, no. 3, pp. 344–350, Aug. 2010.

[6] K. Staszek, I. Piekarz, J. Sorocki, S. Koryciak, K. Wincza, and S. Gruszczynski, "Low-cost microwave vector system for liquid properties monitoring," *IEEE Trans. Ind. Electron.*, vol. 65, no. 2, pp. 1665–1674, Feb. 2018.

[7] A. Omer, G. Shaker, S. Safavi-Naeini, H. Kokabi, G. Alquié, F. Deshours, and R. M. Shubair, "Low-cost portable microwave sensor for non-invasive monitoring of blood glucose level: Novel design utilizing a four-cell CSRR hexagonal configuration," *Sci. Rep.*, vol. 10, no. 15200, pp. 1–20, Sep. 2020.

[8] K. Staszek, A. Szkudlarek, M. Kawa, and A. Rydosz, "Microwave system with sensor utilizing GO-based gas-sensitive layer and its application to acetone detection," *Sens. Actuators B, Chem.*, vol. 297, no. 126699, pp. 1–10, Jun. 2019.

[9] T. D. C. Minh, D. R. Blake, and P. R. Galassetti, "The clinical potential of exhaled breath analysis for diabetes mellitus," *Diabetes Res. Clin. Pract.*, vol. 97, no. 2, pp. 195–205, Aug. 2012.

[10] C. Wang, A. Mbi, and M. Shepherd, "A study on breath acetone in diabetic patients using a cavity ringdown breath analyzer: Exploring correlations of breath acetone with blood glucose and glycohemoglobin A1C," *IEEE Sensors J.*, vol. 10, no. 1, pp. 54–63, Jan. 2010.

[11] J. Sorocki, A. Rydosz, and K. Staszek, "Wideband microwave multiport-based system for low gas concentration sensing and its application for acetone detection," *Sens. Actuators B, Chem*, vol. 323, no. 128710, pp. 1–12, Aug. 2020.

[12] M. H. Zarifi, M. Rahimi, M. Daneshmand, and T. Thundat, "Microwave ring resonator-based non-contact interface sensor for oil sands applications," *Sens. Actuators B, Chem.*, vol. 224, pp. 632–639, Mar. 2016.

[13] M. Shete, M. Shaji, and M. J. Akhtar, "Design of a coplanar sensor for RF characterization of thin dielectric samples," *IEEE Sensors J.*, vol. 13, no. 12, pp. 4706–4715, Dec. 2013.

[14] I. Piekarz, J. Sorocki, K. Wincza, and S. Gruszczynski, "Microwave sensor for dielectric sample measurement based on coupled-line section," *IEEE Trans. Microw. Theory Techn.*, vol. 65, no. 5, pp. 1615–1631, May 2017.

[15] M. A. Stuchly and S. S. Stuchly, "Coaxial line refection methods for measuring dielectric properties of biological substances at radio and microwave frequencies—A review," *IEEE Trans. Instrum. Meas.*, vol. 29, no. 3, pp. 176–183, Sep. 1980.

[16] J. Roelvink, S. Trabelsi, and S. O. Nelson, "A planar transmission-line sensor for measuring the microwave permittivity of liquid and semisolid biological materials," *IEEE Trans. Instrum. Meas.*, vol. 62, no. 11, pp. 2974–2982, Nov. 2013.

[17] A. Ebrahimi, W. Withayachumnankul, S. Al-Sarawi, and D. Abbott, "High-sensitivity metamaterial-inspired sensor for microfluidic dielectric characterization," *IEEE Sensors J.*, vol. 14, no. 5, pp. 1345–1351, May 2014.

[18] S. O. Tatu, A. Serban, M. Helaoui, and A. Koelpin, "Multiport technology: The new rise of an old concept," *IEEE Microw. Mag.*, vol. 15, no. 7, pp. 34–44, Nov. 2014.

[19] A. Koelpin, G. Vinci, B. Laemmle, D. Kissinger, and R. Weigel, "The six-port in modern society," *IEEE Microw. Mag.*, vol. 11, no. 7, pp. 35–43, Dec. 2010.

[20] K. Staszek, S. Gruszczynski, and K. Wincza, "Six-port reflectometer providing enhanced power distribution," *IEEE Trans. Microw. Theory Techn.*, vol. 64, no. 3, pp. 939–951, Mar. 2016.

[21] G. F. Engen, "A (historical) review of the six-port measurement technique," *IEEE Trans. Microw. Theory Techn.*, vol. 45, no. 12, pp. 2414–2417, Dec. 1997.

[22] G. Vinci, S. Lindner, F. Barbon, S. Mann, M. Hofmann, A. Duda, R. Weigel, and A. Koelpin, "Six-port radar sensor for remote respiration rate and heartbeat vital-sign monitoring," *IEEE Trans. Microw. Theory Techn.*, vol. 61, no. 5, pp. 2093–2100, May 2013.

[23] N. S. Chung, J. H. Kim, and J. Shin, "A dual six-port automatic network analyzer and its performance," *IEEE Trans. Microw. Theory Techn.*, vol. MTT-32, no. 12, pp. 1683–1686, Dec. 1984.

[24] S. Jia, "New application of a single six-port reflectometer," *Electron. Lett.*, vol. 20, no. 22, pp. 920–922, Oct. 1984.

[25] K. Staszek, S. Gruszczynski, and K. Wincza, "Broadband measurements of S-parameters utilizing 4×4 Butler matrices," *IEEE Trans. Microw. Theory Techn.*, vol. 61, no. 4, pp. 1692–1699, Apr. 2013.

[26] K. Staszek, S. Gruszczynski, and K. Wincza, "Ultra-wideband dual-line multiprobe reflectometer," *IEEE Trans. Microw. Theory Techn.*, vol. 65, no. 4, pp. 1324–1333, Apr. 2017.

[27] B. Laemmle, G. Vinci, L. Maurer, R. Weigel, and A. Koelpin, "A 77-GHz SiGe integrated six-port receiver front-end for angle-of arrival detection," *IEEE J. Solid-State Circuits*, vol. 47, no. 9, pp. 1966–1973, Sep. 2012.

[28] K. Kim, N. Kim, S.-H. Hwang, Y.-K. Kim, and Y. Kwon, "A miniaturized broadband multi-state reflectometer integrated on a silicon MEMS probe for complex permittivity measurement of biological material," *IEEE Trans. Microw. Theory Techn.*, vol. 61, no. 5, pp. 2205–2214, May 2013.

[29] R. Mirzavand, M. M. Honari, and P. Mousavi, "Direct-conversion sensor for wireless sensing networks," *IEEE Trans. Ind. Electron.*, vol. 64, no. 12, pp. 9675–9682, Dec. 2017.

[30] S. Julrat and S. Trabelsi, "Portable six-port reflectometer for determining moisture content of biomass material," *IEEE Sensors J.*, vol. 17, no. 15, pp. 4814–4819, Aug. 2017.

[31] A. L. de Souza Rolim, A. J. Belfort de Oliveira, and M. T. de Melo, "Six-port complex permittivity measurements," in *Proc. Eur. Microw. Conf.*, Manchester, U.K., Sep. 2006, pp. 492–494.

[32] M. Hofmann, S. Linz, R. Weigel, G. Fischer, and D. Kissinger, "A multiband 2-port VNA for biomedical applications based on two six-port-junctions," in *IEEE MTT-S Int. Microw. Symp. Dig.*, Seattle, WA, USA, Jun. 2013, pp. 1–4.

[33] K. Haddadi and T. Lasri, "Formulation for complete and accurate calibration of six-port reflectometer," *IEEE Trans. Microw. Theory Techn.*, vol. 60, no. 3, pp. 574–581, Mar. 2012.

[34] J. D. Hunter and P. I. Somlo, "An explicit six-port calibration method using five standards," *IEEE Trans. Microw. Theory Techn.*, vol. MTT-33, no. 1, pp. 69–72, Jan. 1985.

[35] J. D. Hunter and P. I. Somlo, "S-parameter measurements with a single six-port," *Electron. Lett.*, vol. 21, no. 4, pp. 157–158, Feb. 1985.

[36] F. Wiedmann, B. Huyart, E. Bergeault, and L. Jallet, "A new robust method for six-port reflectometer calibration," *IEEE Trans. Instrum. Meas.*, vol. 48, no. 5, pp. 927–931, Oct. 1999.

[37] T. Yakabe, M. Kinoshita, and H. Yabe, "Complete calibration of a six-port reflectometer with one sliding load and one short," *IEEE Trans. Microw. Theory Techn.*, vol. 42, no. 11, pp. 2035–2039, Nov. 1994.
[38] C. Will, S. Linz, S. Mann, F. Lurz, S. Lindner, R. Weigel, and A. Koelpin, "Segmental polynomial approximation based phase error correction for precise near field displacement measurements using six-port microwave interferometers," in *Proc. IEEE Topical Conf. Wireless Sensors Sensor Netw. (WiSNet)*, Phoenix, AZ, USA, Jan. 2017, pp. 23–25.
[39] G. F. Engen, "Calibrating the six-port reflectometer by means of sliding terminations," *IEEE Trans. Microw. Theory Techn.*, vol. 26, no. 12, pp. 951–957, Dec. 1978.
[40] S. Linz, G. Vinci, S. Lindner, S. Mann, F. Lurz, F. Barbon, R. Weigel, and A. Koelpin, "I/Q imbalance compensation for six-port interferometers in radar applications," in *Proc. 44th Eur. Microw. Conf.*, Rome, Italy, Oct. 2014, pp. 6–9.
[41] K. Staszek, "Six-port calibration utilizing matched load and unknown calibration loads," *IEEE Trans. Microw. Theory Techn.*, vol. 66, no. 10, pp. 4617–4626, Oct. 2018.
[42] I. Piekarz, J. Sorocki, K. Wincza, and S. Gruszczynski, "Coupled-line sensor with Marchan Balun as RF system for dielectric sample detection," *IEEE Sensors J.*, vol. 16, no. 1, pp. 88–96, Jan. 2016.
[43] S. Odrobina and K. Staszek, "Wideband two-port with programmable scattering parameters," *IET Microw., Antennas Propag.*, vol. 13, no. 14, pp. 2525–2530, Nov. 2019.
[44] K. Staszek, S. Gruszczynski, and K. Wincza, "Theoretical limits and accuracy improvement of reflection-coefficient measurements in six-port reflectometers," *IEEE Trans. Microw. Theory Techn.*, vol. 61, no. 8, pp. 2966–2974, Aug. 2013.

ROBERT SMOLARZ received the M.Sc. degree in electronics and telecommunications with specialization in RF electronics from the Silesian University of Technology, Gliwice, Poland, in 2014. He is currently pursuing the Ph.D. degree with the AGH University of Science and Technology (AGH UST), Kraków, Poland. Since 2015, he has been with AGH UST. He is a member of the Microwave Research Group, Department of Electronics, AGH UST. He has three years of industrial experience in cellular networks development. He has coauthored several journals and conference papers. His current research interests include the development of high-performance microwave passive components utilized in power division circuits and monolithic microwave integrated circuit (MMIC) design.

KAMIL STASZEK received the M.Sc., Ph.D., and D.Sc. (Habilitation) degrees in electronics engineering from the AGH University of Science and Technology, Kraków, Poland, in 2011, 2015, and 2019, respectively. He is currently an Associate Professor with the Department of Electronics, AGH University of Science and Technology. He has more than two years of industrial experience in automotive radars development. He has coauthored over 70 journal and conference scientific papers. His main scientific interests include multiport measurement techniques in sensor applications and design of broadband passive components. He is a member of the Technical Program Committee of the International Conference on Microwaves, Radar, and Wireless Communications (MIKON) and the Junior Vice-Chair of the Polish Section of the International Union of Radio Science (URSI)—Commission A.

KRZYSZTOF WINCZA received the M.Sc. and Ph.D. degrees in electronics and electrical engineering from the Wroclaw University of Technology, Wroclaw, Poland, in 2003 and 2007, respectively, and the D.Sc. degree (Habilitation) from the AGH University of Science and Technology, Kraków, Poland, in 2012. In 2007, he joined the Institute of Telecommunications, Teleinformatics and Acoustics, Wroclaw University of Technology. Since 2009, he has held the position of an Assistant Professor at the Department of Electronics, AGH University of Science and Technology. In 2012, he attended the training program at Stanford University, USA. He has coauthored over 40 journal articles and over 50 scientific conference papers. His current research interest includes analysis and development of microwave passive devices, such as ultrabroadband directional couplers, microstrip antenna arrays, composite right–left-handed artificial transmission lines, and multiport reflectometers. From 2014 to 2019, he was a member of the Editorial Board of the IEEE Microwave and Wireless Components Letters and the Technical Program Committee of the International Conference on Microwaves, Radar, and Wireless Communications (MIKON). He was a recipient of The Youth Award presented at the 10th National Symposium of Radio Sciences (URSI) and the Young Scientist Grant awarded by the Foundation for Polish Science, in 2001 and 2008, respectively. He served as an Expert for the European Union COST 284 Project from 2003 to 2006 and the Polish National Science Center from 2012 to 2014.

SLAWOMIR GRUSZCZYNSKI (Member, IEEE) received the M.Sc. and Ph.D. degrees in electronics and electrical engineering from the Wroclaw University of Technology, Wroclaw, Poland, in 2001 and 2006, respectively. From 2001 to 2006, he was with the Telecommunications Research Institute, Wroclaw. From 2005 to 2009, he was with the Institute of Telecommunications, Teleinformatics, and Acoustics, Wroclaw University of Technology. In 2009, he joined the Faculty of Informatics, Electronics, and Telecommunications, AGH University of Science and Technology, Krakow, where he became the Head of the Department of Electronics, in 2012. He has coauthored more than 40 journals and more than 50 conference scientific papers. He is also a member of the Young Scientists Academy at the Polish Academy of Sciences (PAN) and the Committee of Electronics and Telecommunications at PAN.